Biosensors

International Edition: DOI: 10.1002/anie.201606742
German Edition: DOI: 10.1002/ange.201606742

Alpha-Helical Fragaceatoxin C Nanopore Engineered for Double-Stranded and Single-Stranded Nucleic Acid Analysis

Carsten Wloka, Natalie Lisa Mutter, Misha Soskine, and Giovanni Maglia**

Abstract: *Nanopores are used in single-molecule DNA analysis and sequencing. Herein, we show that Fragaceatoxin C (FraC), an α-helical pore-forming toxin from an actinoporin protein family, can be reconstituted in sphingomyelin-free standard planar lipid bilayers. We engineered FraC for DNA analysis and show that the funnel-shaped geometry allows tight wrapping around single-stranded DNA (ssDNA), resolving between homopolymeric C, T, and A polynucleotide stretches. Remarkably, despite the 1.2 nm internal constriction of FraC, double-stranded DNA (dsDNA) can translocate through the nanopore at high applied potentials, presumably through the deformation of the α-helical transmembrane region of the pore. Therefore, FraC nanopores might be used in DNA sequencing and dsDNA analysis.*

Nanopores have emerged as a powerful approach for single-molecule monitoring of chemical[1] and enzymatic reactions,[2,3] detection of proteins,[4–6] as well as detection and sequencing of nucleic acids.[7–9] Phi29[10] as well as ClyA[11] have been shown to allow translocation of double stranded DNA. Recently, aerolysin was used to discriminate between adenine homopolymers of different lengths.[12] To date, only αHL[13] and MspA[14] have been shown to discriminate nucleic acids. Both nanopores have β-sheets in their transmembrane region. When DNA is threaded through MspA, the current blockade levels are affected by four or more nucleotides[14] while αHL has three sensing zones in its barrel-shaped structure, which accommodates about 20 nucleobases.[13] Thus, new nanopores with different structures and recognition sites may offer improvements in sequencing accuracy or provide different error profiles. Recently, the crystal structure of the octameric FraC pore-forming toxin in complex with sphingomyelin was solved[15] and revealed a funnel-shaped geometry composed of α-helices with a well-defined single constriction point. Here, we describe the reconstitution of pre-oligomerized FraC into planar lipid bilayers composed of 1,2-diphytanoyl-*sn*-glycero-3-phosphocholine (DPhPC) only. While wild-type FraC did not capture DNA, we engineered a FraC version that permitted capture and translocation of ssDNA and discriminated homopolymers of adenine, thymine, and cytosine immobilized with neutravidin. Strikingly, dsDNA could be translocated through FraC, most probably through the elastically deformed α-helical constriction of the nanopore.

Recombinant wild-type FraC protein monomers, genetically fused to a His_6-tag at the C-terminus, were expressed in a BL21(DE3) *E. coli* strain. Previous works established that the pore assembly of actinoporins is triggered by the presence of sphingomyelin in lipid bilayers.[15–18] In agreement, water-soluble monomers of WtFraC purified by Ni-NTA chromatography did not form pores in DPhPC planar lipid bilayers. Therefore, we pre-oligomerized monomers with DPhPC:sphingomyelin (1:1) liposomes. After solubilization of the liposomes in 0.6 % *N*,*N*-dimethyldodecylamine *N*-oxide (LDAO), to prevent the dissociation of the oligomers,[19] LDAO was exchanged to 0.02 % β-dodecyl maltoside (DDM) by a second round of Ni-NTA chromatography (Supporting Information). The addition of sub-microgram quantities of oligomeric WtFraC (WtFraC, Figure 1 A,B, top) in 0.02 % DDM to the *cis* side of the DPhPC planar lipid bilayer readily yielded pores. Distribution of unitary channel conductance for WtFraC pores at ± 50 mV in 1 M NaCl, 15 mM Tris-HCl pH 7.5 buffer, revealed chiefly a single conductance type (Figures 1 C and S1A, top), presumably corresponding to the octamer observed in the recently determined crystal structure.[15] Similar to other biological nanopores, WtFraC channels showed an asymmetric current–voltage (*I*–*V*) relationship (Figure S1B), allowing for the determination of the orientation of the pore. An example trace, obtained in 3 M NaCl, 15 mM Tris-HCl pH 7.5 buffer, is shown in Figure 1 D.

The crystal structure of octameric WtFraC suggests that this nanopore is large enough to allow the threading of ssDNA (1.2 nm constriction diameter).[15] However, in our initial experiments we could not observe ssDNA blockades, most likely because of the negatively charged constriction region of the WtFraC pore preventing DNA translocation.[20,21] To permit the threading of ssDNA through FraC, we substituted aspartate 10 with arginine, producing a nanopore with a positively charged constriction (Figure 1 B, bottom). Because D10R FraC showed a low pore-forming activity (Figure S2), we performed random mutagenesis on the background of the D10R FraC gene and screened the hemolytic activity of the obtained variants (Supporting Information). As a result, we identified the compensatory mutation lysine 159 to glutamic acid (K159E), which is located on the outer rim of the wide vestibule (Figure 1 A). The double mutant D10R/K159E of FraC (ReFraC) displayed nearly wild-type-levels of hemolytic activity (Figure S2) and yielded uniform pores (Figure 1 C), albeit with an altered *I*–*V* relationship compared to WtFraC (Figure S1B

[*] Dr. C. Wloka, N. L. Mutter, Dr. M. Soskine, Prof. Dr. G. Maglia
Chemical Biology I, Groningen Biomolecular Sciences and Biotechnology Institute (GBB)
University of Groningen
9747 AG, Groningen (The Netherlands)
E-mail: m.soskine@rug.nl
g.maglia@rug.nl

Supporting information and the ORCID identification number(s) for the author(s) of this article can be found under http://dx.doi.org/10.1002/anie.201606742.

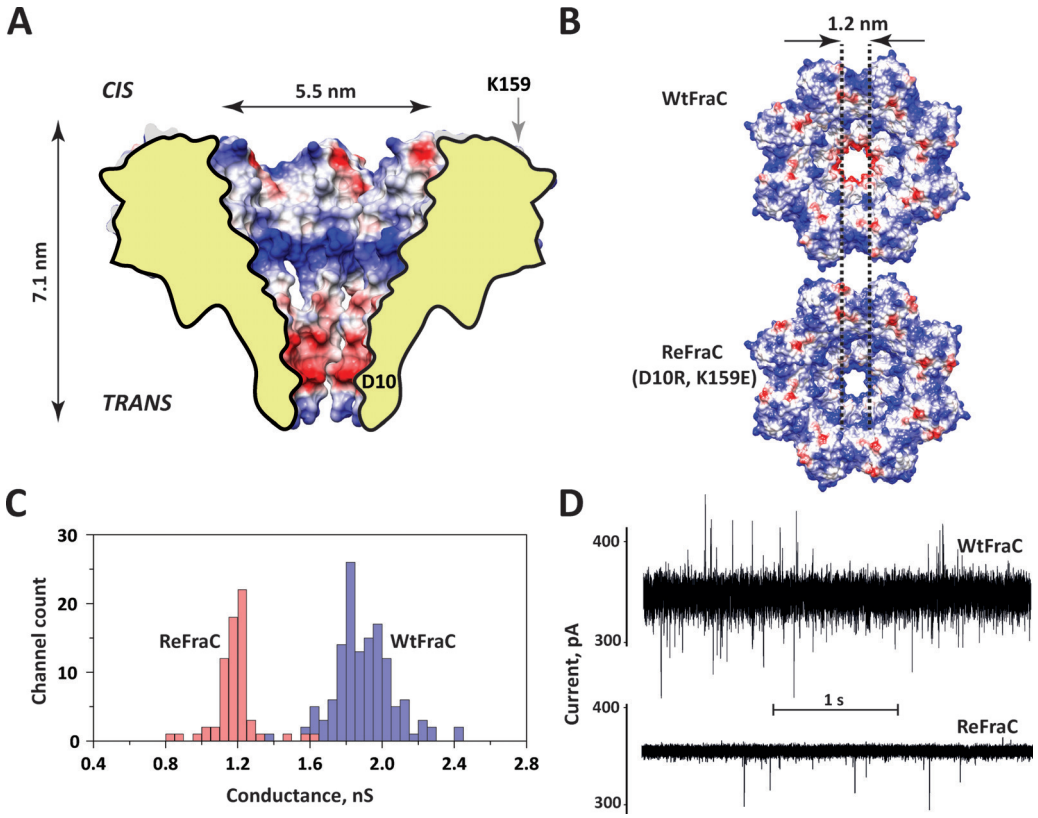

Figure 1. Wild-type FraC (WtFraC) and D10R/K159E FraC (ReFraC) nanopores. A) Cross-section through octameric WtFraC showing Coulombic surface coloring (red = negative charges, blue = positive charges) created with Chimera (University of California, San Francisco). Aspartate 10 is located in the constriction zone and lysine 159 is located on the outer rim of the wide vestibule (arrow) of WtFraC. B) Top view on WtFraC (top) and ReFraC (bottom). C) Single-channel conductance histogram for WtFraC (blue) and ReFraC (red) at +50 mV in 1 M NaCl, 15 mM Tris-HCl, pH 7.5. D) Raw trace of WtFraC (top) and ReFraC (bottom) at +100 mV in 3 M NaCl, 15 mM Tris-HCl, pH 7.5 buffer obtained with identical acquisition settings (2 kHz low-pass Bessel filter and 10 kHz sampling rate).

and Figure 1 D). The lower conductance of ReFraC pores at ±50 mV in 1M NaCl, 15 mM Tris-HCl, pH 7.5 buffer can be attributed to a narrower constriction as arginine has a bulkier side chain than aspartate (Figure 1 B).

Next, we followed established approaches with αHL[13,22–24] and MspA[21,25] to immobilize DNA with neutravidin (NA) because free ssDNA translocated through ReFraC too quickly for thorough analysis (Figure S3). We complexed 5′-end biotinylated $A_{20}/C_{20}/T_{20}$ ssDNA homopolymers with tetrameric NA to assess the ability of ReFraC to translocate and discriminate DNA strands. We added premixed DNA (1 μM) and NA (0.25 μM) to the *cis* compartment of the planar lipid bilayer setup and performed DNA discrimination experiments in 3 M NaCl, 15 mM Tris-HCl, pH 7.5 buffer and +70 mV applied potential (referring to the *trans* electrode). We observed permanent current blockades, which are caused by pseudorotaxanes when ssDNA is stably threaded through the pore until the applied potential is reversed (Figure 2 A). The residual currents, I_{res}, which are the percentage ratios of the amplitudes of blocked and open pore currents multiplied by 100 ($((I_B/I_O)\times 100)$ were: 13.1 ± 0.4 % for NA:A_{20} (N = 5, n = 364, where N is the number of independent single-pore experiments and n the analyzed blockades), 10.8 ± 0.3 % (N = 4, n = 920) for NA:C_{20} and 14.0 ± 0.3 % (N = 5, n = 780) for NA:T_{20} (Figure 2 B). To exclude effects of pore-to-pore variation, we also resolved mixtures of homopolymers (Figure 2 C–F). The relatively low residual currents suggest a tight closure of the pore around threaded ssDNA. We also tried to discriminate between nucleotides containing stretches of G, however, because polyG forms stable secondary structures, the results were inconclusive (Figure S4).

The constriction of ReFraC (1.2 nm) is smaller than the diameter of the B-form of double-stranded DNA (dsDNA, ≈2 nm). Thus, to evaluate dsDNA as a stopper for DNA analysis, we designed two oligonucleotides: oligo I with a biotin group attached at the 5′-terminus with the sequence bio-5′-A_{20}-GTGCTACGACTCTCTGTGTG-C_{20}-3′, and a shorter oligo II with reverse complement sequence to the underlined part of oligo I. Annealing yielded an A_{20}-$(dsDNA)_{20}C_{20}$ substrate. Addition of 1 μM of A_{20}-$(dsDNA)_{20}C_{20}$ to the *cis* compartment at +50 mV caused transient blockades to the ReFraC pore (blockade lifetime 2 ± 5 s, I_{res} = 10.0 ± 0.2 %, N = 3, n = 290, Figure S5A, left). Increasing the applied potential to +70 mV shortened the blockades lifetimes about thousand-fold to 2.9 ± 0.4 ms (note that the residual currents showed two current levels: 12.8 ± 0.6 % and 3.5 ± 0.5 % N = 3 n = 2700 Figure S5B, left). The decrease of blockade lifetime with the potential suggests the translocation of $A_{20}(dsDNA)_{20}C_{20}$ through ReFraC.[26] To

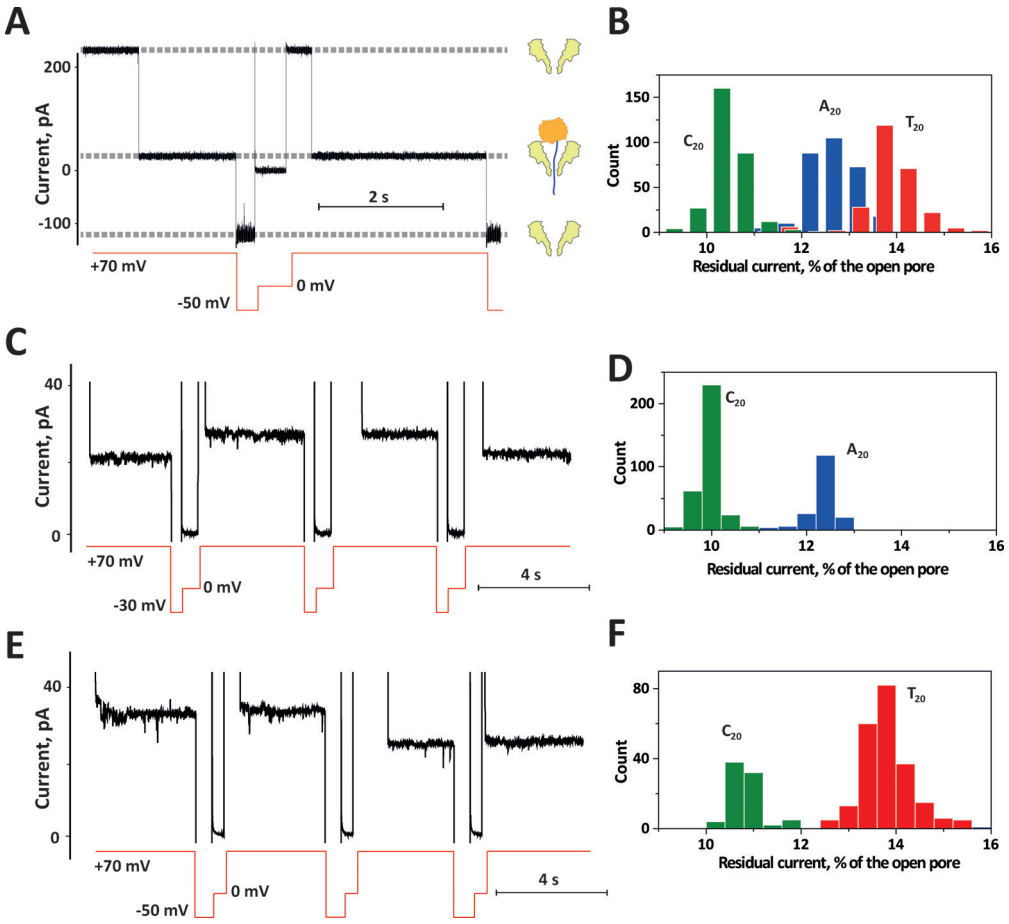

Figure 2. DNA discrimination with ReFraC. A) Representative blockades of a homopolymeric DNA strand in complex with NA using ReFraC. The cartoon shows the interpretation of the current blockades. B) Representative distributions of residual currents obtained for A_{20}, C_{20}, and T_{20} homopolymeric strands with ReFraC nanopores. C) Current blockades of a continuous trace induced by homopolymeric C_{20} and A_{20} nucleotides to the same ReFraC pore. D) Distribution of residual currents imposed by mixtures of C_{20} and A_{20} homopolymeric strands. E) Continuous trace of an experiment to resolve mixtures of homopolymeric C_{20} and T_{20} nucleotides. F) Distribution of residual currents imposed by mixtures of C_{20} and T_{20} homopolymeric strands. Traces were recorded in 3 M NaCl, 15 mM Tris-HCl, pH 7.5, using 2 kHz low-pass Bessel filter and 10 kHz sampling rate. Traces C and E were subjected to additional 100 Hz Gaussian digital filtering. Automatic voltage-stepping procedures are shown below the traces with the red lines.

confirm DNA translocation, we added NA to the *cis* chamber. NA:A_{20}(dsDNA)$_{20}C_{20}$ blockades became permanent both at +50 mV, (Figure S5A, right) and at +70 mV (Figure S5B, right), therefore suggesting that the blockades in the absence of NA could not be released through A_{20}(dsDNA)$_{20}C_{20}$ exiting back to the *cis* compartment. Curiously, at +50 mV, 31 ± 4 % of the NA:A_{20}(dsDNA)$_{20}C_{20}$ blockades ($N = 3$, $n = 468$) showed a stepwise enhancement of the residual current from a transient level (Figure 3 A, state 2, $I_{res} = 8.8 \pm 0.7$ %) to a stable level (Figure 3 A, state 3, with $I_{res} = 12.5 \pm 0.7$ %, $N = 4$, $n = 46$; more examples in Figure S6). The current level of state 2 ($I_{res} = 10.5 \pm 0.7$; $N = 3$, $n = 206$ at +50 mV) was slightly lower than that of NA:C_{20}. The current level of state 3 matched that of NA:A_{20}. A likely explanation for these current enhancements is that at +50 mV the C_{20} segment of NA:A_{20}(dsDNA)$_{20}C_{20}$ is dwelling in the constriction of the nanopore (Figure 3 A, state 2), with the duplex segment preventing the further translocation. However, after the unzipping of the duplex, A_{20} occupies the constriction of ReFraC, with NA arresting the translocation (Figure 3 A, state 3). In agreement with this hypothesis, at +50 mV, NA:A_{20}(dsDNA)$_{20}C_{20}$ blockades were immediately relieved when the potential was reversed to −30 mV, indicating that at +50 mV translocation of A_{20}(dsDNA)$_{20}C_{20}$ is mediated by unzipping (Figure 3 A, brackets). In contrast, at +70 mV, a significant fraction of blockades was not immediately released at −30 mV (Figure 3 B, inset), indicating the formation of an interlocked state (Figure 3 B, states 2 and 3). Further, these interlocked states were generated more frequently with increasing the potential (for example, from 7 ± 4 % of all blockades at +70 mV to 54 ± 14 % at +100 mV, $N = 3$, $n = 739$; Figure 3 B, insert). Considering that blockades of oligo I alone in complex with NA were released immediately at −30 mV (Figure S8A), we attribute such interlocked states to a rotaxane where NA and the duplex DNA segment of A_{20}(dsDNA)$_{20}C_{20}$ serve as *cis* and *trans* stoppers, respectively (Figure 3 B, right). As expected, such rotaxanes could also be formed from NA:oligo I *cis* blockades by adding

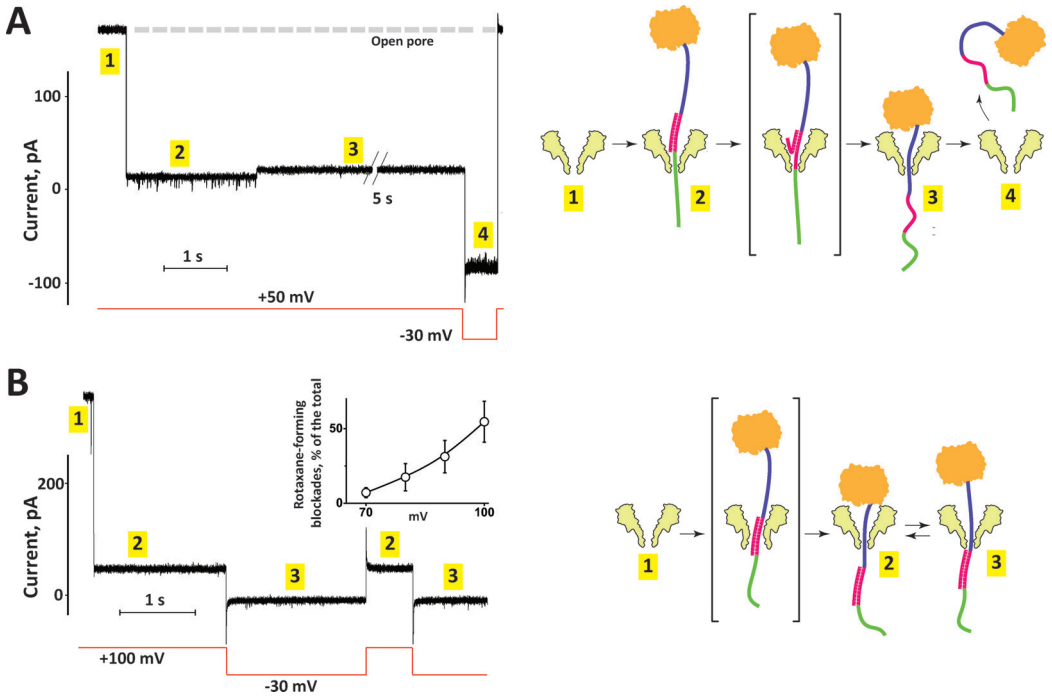

Figure 3. Unzipping/translocation of dsDNA by ReFraC. A) Representative trace of ReFraC capturing a NA:$A_{20}(dsDNA)_{20}C_{20}$ complex at +50 mV. The open pore current is denoted as 1 and indicated by dotted line. Two levels can be observed in the block: firstly, a lower level (2), likely corresponding to the stretch of homopolymeric cytosine which converts through an intermediate level (unzipping, brackets) into a higher level (3), most likely corresponding to the stretch of homopolymeric adenine. Upon reversal of potential (4), the block is immediately released indicating that the double-stranded region NA:$A_{20}(dsDNA)_{20}C_{20}$ complex was peeled off. B) At + 100 mV, a single block is observed (2). In more than half of the cases (insert),the dsDNA part is pushed through (deformation, brackets), and upon application of −30 mV the block cannot be released immediately (3). At higher negative potentials the block can be released, indicating a rotaxane was formed (more examples in Figure S7). Traces were recorded in 3 M NaCl, 15 mM Tris-HCl, pH 7.5, using 2 kHz low-pass Bessel filter and 10 kHz sampling rate.

oligo II in *trans* (Figure S8B). Switching the potential to −40 mV quickly dismantled the rotaxanes, presumably through unzipping of the dsDNA stopper in *trans* (Figure S7 and S8B).

Formation of a rotaxane from NA:$A_{20}(dsDNA)_{20}C_{20}$ present in *cis* requires the deformation of the ReFraC pore to allow the translocation of the duplex segment of the $A_{20}(dsDNA)_{20}C_{20}$ substrate (Figure 3 B, brackets). Previously, we observed that the blockades of human thrombin (≈4.2 nm diameter) to type I ClyA-CS nanopores (≈3.3 nm constriction diameter) were often followed by a transient increase in the open pore current.[27] This phenomenon was interpreted as translocation of the protein through the deformed α-helical constriction of ClyA. Here, we show that the ReFraC transmembrane helices can be deformed to allow the passage of intact dsDNA. Thus, this structural flexibility may be a general feature of α-helical pores.

In conclusion, we devised a method to reconstitute pre-oligomerized FraC nanopores in sphingomyelin-free planar lipid bilayers. The ReFraC nanopore was engineered to allow electrophoretic DNA capture and showed discrimination among ssDNA homopolymers. In contrast to other nanopores used to sequence DNA (such as αHL and MspA), FraC has an α-helical V-shaped transmembrane region that may be advantageous for fine-tuning nucleobase discrimination. This is because amino acids substitutions at different positions within the transmembrane α-helices may modulate both the size and chemical composition of the constriction.

Keywords: DNA analysis · DNA sequencing · fragaceatoxins · nanopores · single-molecule studies

How to cite: *Angew. Chem. Int. Ed.* **2016**, *55*, 12494–12498
Angew. Chem. **2016**, *128*, 12682–12686

[1] T. Luchian, S. H. Shin, H. Bayley, *Angew. Chem. Int. Ed.* **2003**, *42*, 3766–3771; *Angew. Chem.* **2003**, *115*, 3896–3901.
[2] M. M. Mohammad, R. Iyer, K. R. Howard, M. P. McPike, P. N. Borer, L. Movileanu, *J. Am. Chem. Soc.* **2012**, *134*, 9521–9531.
[3] C. W. Ho, V. Van Meervelt, K. C. Tsai, P. J. De Temmerman, J. Mast, G. Maglia, *Sci. Adv.* **2015**, *1*, e1500905.
[4] M. Soskine, A. Biesemans, B. Moeyaert, S. Cheley, H. Bayley, G. Maglia, *Nano Lett.* **2012**, *12*, 4895–4900.
[5] M. Fahie, C. Chisholm, M. Chen, *ACS Nano* **2015**, *9*, 1089–1098.
[6] T. Li, L. Liu, Y. Li, J. Xie, H. C. Wu, *Angew. Chem. Int. Ed.* **2015**, *54*, 7568–7571; *Angew. Chem.* **2015**, *127*, 7678–7681.
[7] J. J. Kasianowicz, E. Brandin, D. Branton, D. W. Deamer, *Proc. Natl. Acad. Sci. USA* **1996**, *93*, 13770–13773.
[8] M. Akeson, D. Branton, J. J. Kasianowicz, E. Brandin, D. W. Deamer, *Biophys. J.* **1999**, *77*, 3227–3233.
[9] H. Y. Wang, Y. Li, L. X. Qin, A. Heyman, O. Shoseyov, I. Willner, Y. T. Long, H. Tian, *Chem. Commun.* **2013**, *49*, 1741–1743.

[10] D. Wendell, P. Jing, J. Geng, V. Subramaniam, T. J. Lee, C. Montemagno, P. Guo, *Nat. Nanotechnol.* **2009**, *4*, 765 – 772.
[11] L. Franceschini, M. Soskine, A. Biesemans, G. Maglia, *Nat. Commun.* **2013**, *4*, 2415.
[12] C. Cao, Y. L. Ying, Z. L. Hu, D. F. Liao, H. Tian, Y. T. Long, *Nat. Nanotechnol.* **2016**, *11*, 713 – 718 .
[13] D. Stoddart, A. J. Heron, E. Mikhailova, G. Maglia, H. Bayley, *Proc. Natl. Acad. Sci. USA* **2009**, *106*, 7702 – 7707.
[14] A. H. Laszlo, I. M. Derrington, B. C. Ross, H. Brinkerhoff, A. Adey, I. C. Nova, J. M. Craig, K. W. Langford, J. M. Samson, R. Daza, K. Doering, J. Shendure, J. H. Gundlach, *Nat. Biotechnol.* **2014**, *32*, 829 – 833.
[15] K. Tanaka, J. M. Caaveiro, K. Morante, J. M. Gonzalez-Manas, K. Tsumoto, *Nat. Commun.* **2015**, *6*, 6337.
[16] A. Barlic, I. Gutierrez-Aguirre, J. M. Caaveiro, A. Cruz, M. B. Ruiz-Arguello, J. Perez-Gil, J. M. Gonzalez-Manas, *J. Biol. Chem.* **2004**, *279*, 34209 – 34216.
[17] B. Bakrac, I. Gutierrez-Aguirre, Z. Podlesek, A. F. Sonnen, R. J. Gilbert, P. Macek, J. H. Lakey, G. Anderluh, *J. Biol. Chem.* **2008**, *283*, 18665 – 18677.
[18] P. Schön, A. J. Garcia-Saez, P. Malovrh, K. Bacia, G. Anderluh, P. Schwille, *Biophys. J.* **2008**, *95*, 691 – 698.
[19] K. Tanaka, J. M. Caaveiro, K. Tsumoto, *Biochemistry* **2015**, *54*, 6863 – 6866.
[20] G. Maglia, M. R. Restrepo, E. Mikhailova, H. Bayley, *Proc. Natl. Acad. Sci. USA* **2008**, *105*, 19720 – 19725.
[21] T. Z. Butler, M. Pavlenok, I. M. Derrington, M. Niederweis, J. H. Gundlach, *Proc. Natl. Acad. Sci. USA* **2008**, *105*, 20647 – 20652.
[22] R. F. Purnell, J. J. Schmidt, *ACS Nano* **2009**, *3*, 2533 – 2538.
[23] D. Stoddart, A. J. Heron, J. Klingelhoefer, E. Mikhailova, G. Maglia, H. Bayley, *Nano Lett.* **2010**, *10*, 3633 – 3637.
[24] D. Stoddart, G. Maglia, E. Mikhailova, A. J. Heron, H. Bayley, *Angew. Chem. Int. Ed.* **2010**, *49*, 556 – 559; *Angew. Chem.* **2010**, *122*, 566 – 569.
[25] E. A. Manrao, I. M. Derrington, M. Pavlenok, M. Niederweis, J. H. Gundlach, *PLoS One* **2011**, *6*, e25723.
[26] A. Biesemans, M. Soskine, G. Maglia, *Nano Lett.* **2015**, *15*, 6076 – 6081.
[27] M. Soskine, A. Biesemans, M. De Maeyer, G. Maglia, *J. Am. Chem. Soc.* **2013**, *135*, 13456 – 13463.

Received: July 12, 2016
Published online: September 8, 2016

